HYDROLOGICAL PROCESSES
Hydrol. Process. **28**, 6337–6350 (2014)
Published online 12 December 2013 in Wiley Online Library
(wileyonlinelibrary.com) DOI: 10.1002/hyp.10118

Assessing the influence of the Merzbacher Lake outburst floods on discharge using the hydrological model SWIM in the Aksu headwaters, Kyrgyzstan/NW China

M. Wortmann,[1,2]* V. Krysanova,[1] Z. W. Kundzewicz,[1,3] B. Su[4] and X. Li[4]

[1] *Potsdam Institute for Climate Impact Research, Telegraphenberg A31, P.O. Box 601203, 14412, Potsdam, Germany*
[2] *UCL, Department of Geography, University College London, Pearson Building, Gower Street, London WC1E 6BT, UK*
[3] *Institute for Agricultural and Forest Environment of Polish Academy of Sciences, Ul. Bukowska 19, 60-809, Poznań*
[4] *Chinese Meteorological Administration, National Climate Centre, No. 46, Zhongguancun South Street, Haidian District, Beijing, China*

Abstract:

Glacial lake outburst floods (GLOF) often have a significant impact on downstream users. Including their effects in hydrological models, identifying past occurrences and assessing their potential impacts are challenges for hydrologists working in mountainous catchments. The regularly outbursting Merzbacher Lake is located in the headwaters of the Aksu River, the most important source of water discharge to the Tarim River, northwest China. Modelling its water resources and the evaluation of potential climate change impacts on river discharge are indispensable for projecting future water availability for the intensively cultivated river oases downstream of the Merzbacher Lake and along the Tarim River. The semi-distributed hydrological model SWIM was calibrated to the outlet station Xiehela on the Kumarik River, by discharge the largest tributary to the Aksu River. The glacial lake outburst floods add to the difficulties of modelling this high-mountain, heavily glaciated catchment with poor data coverage and quality. The aims of the study are to investigate the glacier lake outburst floods using a modelling tool. Results include a two-step model calibration of the Kumarik catchment, an approach for the identification of the outburst floods using the measured gauge data and the modelling results and estimations of the outburst flood volumes. Results show that a catchment model can inform GLOF investigations by providing 'normal' (i.e. without the outburst floods) catchment discharge. The comparison of the simulated and observed discharge proves the occurrence of GLOFs and highlights the influences of the GLOFs on the downstream water balance. © 2013 The Authors. *Hydrological Processes* Published by John Wiley & Sons Ltd.

KEY WORDS GLOF; jökulhlaup; Aksu River; Tarim River; Soil and Water Integrated Model; Merzbacher Lake

Received 17 June 2013; Accepted 13 November 2013

INTRODUCTION

Hydrological modelling for climate change impact assessment of mountainous catchments is challenged by complex physical conditions and data availability that introduce large uncertainty ranges (Gurtz *et al*., 2003; Moussa *et al*., 2007). Most commonly, data have poor coverage and quality at high altitudes requiring extrapolation over large topographically heterogeneous areas and elevation zones. Also, complex hydrological processes such as snow and glacier melt paired with data scarcity require catchment models to compromise physical for more empirical representations (Wagener *et al*., 2004)..

The Aksu River, originating in the Tian Shan mountains in Kyrgyzstan, is the largest and principal tributary to the endorheic Tarim River in northwest China, providing 70–80% of its total water flow (Wang *et al*., 2008). The Tarim provides water to the arid to hyperarid Xinjiang Uyghur Autonomous Region in China (hereafter referred to as Xinjiang), including irrigated oases along lowland river courses. Due to increased water demand resulting from the extension of cultivated areas in the region since the 1950s, the 320 km long lower reach of the Tarim fell dry and two terminal lakes disappeared (Thevs, 2011). This study focuses on the headwater part of the Aksu delineated by the catchment of the gauging station Xiehela, where the river is called Kumarik.

Approximately 45% of the total discharge of the Tarim is generated in the Kumarik catchment, the Aksu River's largest headwater tributary in terms of water discharge. Consequently, any changes in this catchment (e.g. due to a warmer and wetter climate as has been suggested by Shi *et al*., 2006) are likely to have significant influence on the downstream Tarim River. Located in the Tian Shan mountain range at altitudes above 1434 m asl, the catchment is dominated by snow and glacier melt paired

*Correspondence to: Michel Wortmann, Climate Impacts & Vulnerabilities, Potsdam Institute for Climate Impact Research, Telegraphenberg A31, P.O. Box 601203, 14412 Potsdam, Germany.
E-mail: wortmann@pik-potsdam.de

with orographic precipitation during spring and summer. Existing studies (Pieczonka *et al*., 2013 Osmonov *et al*., 2013 and review in Krysanova *et al*., 2013, submitted) show that glaciers in the Aksu basin show on average an area and mass loss during the last decade but the loss was not spatially and temporally homogeneous.

Only few high-altitude climate stations exist in or close to the Kumarik catchment, and river gauging stations are sparse and biased by bank freezing. Climate change impact assessments of the headwater parts of the Aksu basin have become important for the intensively used arid downstream regions of the Aksu and Tarim rivers. However, the complex glacier processes and poor data availability make this a difficult task.

The Aksu River experiences reoccurring glacier lake outburst floods (GLOFs) produced by the Merzbacher Lake located in the Inylchek valley in Kyrgyzstan at an altitude of 3250 m asl., ca. 200 km upstream of Xiehela gauging station (see review in Glazirin, 2010). The outbursts usually occur at the end of summer or beginning of autumn, with peak floods at the Xiehela station (see Figure 1) exceeding 1000 m^3s^{-1}, i.e. 6.5 the mean annual discharge (151 m^3s^{-1} based on data from 1964–1987) or 2.5 times the mean summer discharge (JJA, 406 m^3s^{-1} in the same period). These floods have proven destructive to downstream communities, infrastructure as well as agricultural and industrial land in the Aksu-Tarim region. Research has become vital in providing information about the floods and their future development under a warming climate (Liu, 1992; Shen *et al*., 2009).

Glazirin (2010) lists recorded GLOF events during the last 80 years compiled from various sources in his review of the Merzbacher Lake. The list of reported events, however, has many gaps in years where GLOFs were not reported. The only long-term hydrological record of the floods is provided by the Xiehela hydrological station.

Liu (1992) visually identified and characterized the GLOFs from the Merzbacher Lake using the Xiehela hydrological records. Flood volumes were estimated via graphical hydrograph separation and an empirical exponential equation was developed to simulate the rising limb of the hydrograph. The analysis, however, was not based on the discharge that would have occurred in the absence of outburst floods from the Merzbacher Lake (hereafter referred to as 'normal discharge') creating inaccuracies in the graphical identification (see also Ng and Liu, 2009).

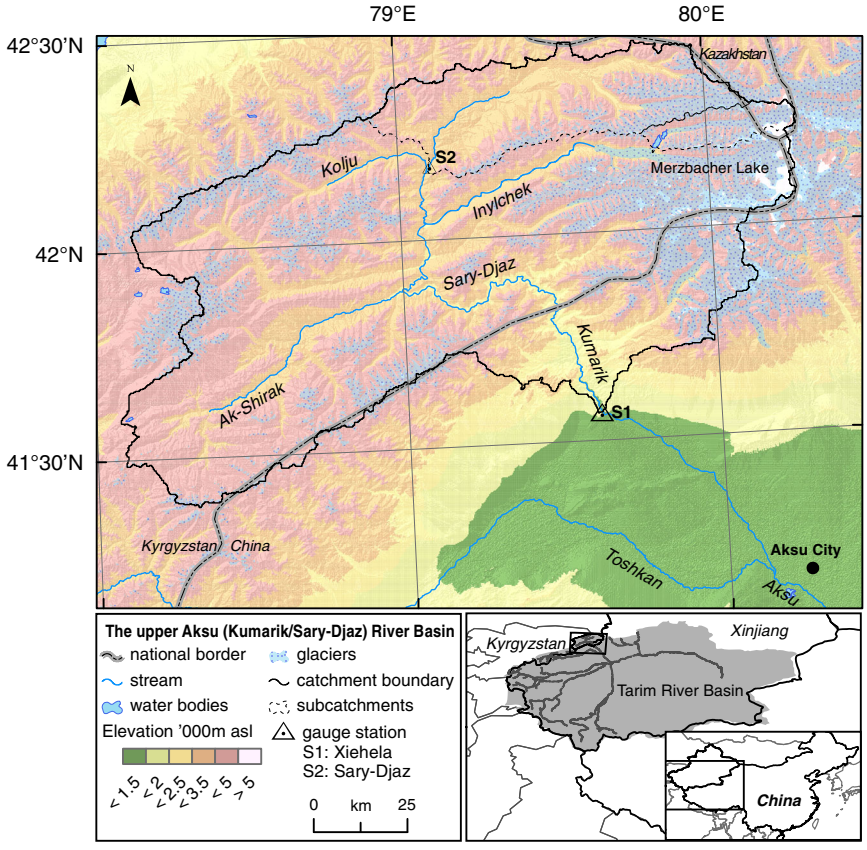

Figure 1. The upper Aksu River Basin, the headwater reaches are called Sary-Djaz River in Kyrgizstan and Kumarik River in China. The outlet station Xiehela records approx. Sixty-four percent of the Aksu River discharge and by that roughly 45% of the Tarim River

Most GLOFs occur during the receding limb of the high summer discharge in late August or September. Thus, the outbursting water adds to a dynamic catchment discharge. The normal catchment discharge is needed to act as baseflow for accurate hydrograph separation for GLOF periods.

The hydrological and climatic controls of the Merzbacher Lake outburst floods are still unclear. Ng *et al*. (2007) inferred melt water supply during the flood events to the lake via inversion of the Nye subglacial drainage equations taking into account peak discharge and graphically inferred flood volumes. Correlations of the melt water supply with daily surface temperature averaged over the first third of the flood period at lake level ($r^2 = 0.77$) and graphically separated baseflow at Xiehela station ($r^2 = 0.86$) were found, suggesting high dependence of peak discharge on prevailing weather conditions. This analysis, however, was only based on half of the observed GLOFs, for which the constraint parameters (peak discharge and volume) could be reliably inferred. They also could not define conditions triggering the outburst. Therefore, modelling the normal catchment discharge at Xiehela would help to achieve a more reliable baseflow separation as well as a better analysis of interdependencies between climate and the hydrological phenomena. Simulating discharge from the Merzbacher Lake catchment can also reveal more about the hydrological conditions leading to the GLOF events.

The aims of this study are (1) to provide a modelling-based analysis on how the GLOFs from the Merzbacher Lake influence river discharge at the Xiehela station in the headwater part of the Aksu River, (2) to suggest an approach for detection of the outburst floods based on the measured gauge data and simulated discharge, and (3) to provide an estimation of the outburst flood volumes. This is achieved by calibrating and validating the process-based, semi-distributed hydrological model SWIM (Soil and Water Integrated Model) for the Kumarik catchment at the Xiehela gauging station, first considering the total observed discharge and second excluding GLOF periods from the observations. Further, it is shown that GLOF events can be detected by considering the simulation residuals (i.e. differences between observed and simulated discharge) and that the outburst flood volume can be determined using the simulated normal flow.

STUDY SITE AND DATA

The Aksu is an important source of water to the Tarim River in Xinjiang. The region has an arid climate (Aizen *et al*., 1995), but glacier and snow melt in the headwaters of the Aksu and its tributaries maintain river flow and provide water resources for the extensive oases of Xinjiang.

The catchment terminated by the Xiehela hydrological station (S1 in Figure 1) defines the model domain with a drainage area of 12 991 km^2. This station provides the only long-term hydrological record of the GLOFs in this region. Most of the catchment area is located in Kyrgyzstan, where the river is called the Sary-Djaz. Downstream of its confluence with the Inylchek and Ak-Shirak rivers, it flows into China, where the river is known by the name Kumarik, and after joining the Toshkan River, it is called the Aksu River (see Figure 1).

The highly glaciated Kumarik catchment ranges from 1434 m asl at its outlet to 7127 m asl at its highest peak, the Jengish Chokuso in Kyrgyz (or Pik Pobedy in Russian or Tömür in Uyghur). One subcatchment (delineated by the station S2, see Figure 1) is terminated by a gauging station on the Sary-Djaz River for which discharge data are available. Table I provides details of the entire catchment, the internal subcatchment and the ungauged Merzbacher Lake subcatchment. With mean winter and summer discharge of 28 m^{3}s^{-1} (DJF) and 406 m^{3}s^{-1} (JJA) for the study period 1964–1987, the Kumarik catchment has a pronounced nival regime. Warm and moist frontal systems from the west trigger both snow and glacier melt and orographic rain during summer (Aizen *et al*., 1995). Daily mean (min., max.) temperatures averaged over the catchment range from −17 °C (−23, −10) in winter to 7 °C (1, 15) in summer with a mean monthly precipitation of 7 mm and 50 mm in winter and summer, respectively.

In a rare physiographical setting, the Merzbacher Lake is located between the Northern Inylchek and the much larger Southern Inylchek glacier at an elevation of 3250 m (79°52′*E*, 42°13′*N*). The northern glacier provides most of the discharge to the lake, while the southern glacier acts as a perpendicular dam to the lake with a valley-blocking tongue reaching into the lake. In the event of an outburst, this tongue floats up triggering the subglacial channels to

Table I. Catchment details according to the four hydrological stations and the Merzbacher Lake; drainage area, mean discharge Q as annual mean and summer mean for the month June to August (over 1964–1987) and glacier cover. See Table II for sources

Station	River	Area [km^2]	Mean Q [m^{3}s^{-1}]	Mean JJA Q [m^{3}s^{-1}]	Glacier [%]
S1	Kumarik R.	12 991	151.8	406.6	22
S2	Sary-Djaz R.	1927	37.4	91.3	18
Merzbacher L.	Enylchek R.	325			55

widen in turn emptying the lake. First discovered by Gottfried Merzbacher in 1903 (Merzbacher, 1905), Merzbacher Lake has since been known to outburst almost every year and in some years even twice, mostly in the period from July to October (Glazirin, 2010). The lake has split into an upper and a lower part with a difference in elevation of 100 m divided by a 2–3 km field of debris.

Investigating possible trigger mechanisms, predicting peak discharges and flood volumes and, by that, predicting the occurrence of the floods have become the focus of discussion about the Merzbacher Lake GLOFs (Glazirin, 2010). Ajrapetyants and Bakov (1971) proposed the so far unverified hypothesis that the lake empties once the water volume is able to float the damming part of the Southern Inylchek glacier. Cracks and crevasses then open up to form englacial channels which are enlarged by the slightly warmer lake water, a self-accelerating process fueled by the increasing kinematic energy. Once the lake water is drained through the Southern Inylchek glacier tongue, the dam and channels close again and the lake refills. Validation of this hypothesis has so far been limited by accessibility for measurements. Detailed understanding of the interplay between glacier dynamics and lake volumes is therefore lacking.

Uncertainty over Merzbacher Lake GLOF occurrence, peak discharge and volume increases in view of the general increase in temperature and precipitation in the Tian Shan. It is suggested that this trend may lead to more frequent and higher magnitude GLOFs in the entire Tarim catchment (Shen *et al.*, 2009). Merzbacher Lake GLOFs have been found to occur earlier in the year compared to the 1930s. It has also been suggested that peak discharges have increased (Liu and Fukushima, 1999; Ng *et al.*, 2007; Glazirin, 2010).

An overview of the data used for the model and their sources is given in Table II. The model is driven by six climate variables: mean, maximum and minimum temperature, precipitation, relative humidity and solar radiation. The climate data were assimilated from two sources: (1) the Water and Global Change (WATCH) project dataset, a reanalysis dataset created for hydrological investigations, and (2) a gridded dataset supplied by the Chinese Meteorological Administration (CMA), created by interpolation with elevation correction of observed data from meteorological stations. Temperature and precipitation for the Kyrgyz part of the catchment as well as relative humidity and solar radiation for the entire catchment were derived from the WATCH dataset, while the CMA dataset provided temperature and precipitation for the Chinese part. Reliable climate data for Kyrgyzstan are sparse; the Tian Shan meteorological station data as well as some precipitation records with many gaps were omitted in favour of homogeneity between the gridded datasets.

Table II. Input data used to drive SWIM and to calibrate/validate the model. Topography and glaciers are shown in Figure 1. Climate variables are: temperature T (mean, min., max.), precipitation P, radiation and relative humidity

Data	Source
Climate	WATCH (Weedon *et al.*, 2011), 0.5º grid points for T and P were used for the Kyrgyz part and radiation and relative humidity for the entire model domain. T and P for the Chinese part were supplied by the Chinese Meteorological Administration as interpolated 0.25º grid cells.
Topography	SRTM hole-filled digital elevation model at 90 m resolution (Jarvis *et al.*, 2007)
Land cover	Chinese Meteorological Administration for Chinese part, MODIS 500 m land cover (2001) (Friedl *et al.*, 2002) for Kirghiz part, reclassified to SWIM land cover classes
Glaciers	Improved GLIMS glacier distribution with individual glacier delineation by Bolch *et al.* (2012)
Soil	Harmonised World Soil Database (FAO *et al.*, 2011), includes the 1:1 Mil. soil map for China
Discharge	Daily river discharge at gauge Xiehela (S1) from Chinese hydrological year books and Sary-Djaz River (S2) from Kyrgyz hydrological yearbooks (both for the period 1964–87)

Land cover information was derived from the global MODIS Land Cover Type product for the Kyrgyz part of the catchment and from a land cover map provided by the CMA for the Chinese part. Their original classes were reclassified to SWIM land cover classes including a glacier class.

Soil types were provided by the Harmonised World Soil Database (HWSD), which includes the $1 : 10^6$ soil map of China. The properties (mainly particle size distribution) of the dominant soil were used to extend the information to porosity, field and available water capacity as well as hydraulic conductivity using common pedotransfer functions (Woesten *et al.*, 2001).

Individual glaciers outlines were provided by Bolch *et al.* (2012), who improved the Global Land Ice Measurements from Space (GLIMS) database for the Aksu basin. The spatial distributions of glaciers including their individual area are used to estimate their water equivalent volumes (see next section).

Daily river discharge data for the Xiehela gauging station were obtained from the hydrological yearbooks published by the Chinese Ministry of Water Resources. Discharge records from Kyrgyz hydrological yearbooks were used for the Kyrgyz station.

METHODS

The Soil and Water Integrated Model (SWIM)

The process-based ecohydrological model SWIM was implemented for the Kumarik catchment at daily time steps. SWIM is a semi-distributed model for meso-scale to large catchments, simulating all important hydrological processes, including snow and glacier melt. SWIM was developed from the Soil and Water Assessment Tool (SWAT) (Arnold *et al*., 1993) and MATSALU (Krysanova *et al*., 1989) as a tool for climate and land use change assessments. It was first applied for the Elbe River in northern Germany (Krysanova *et al*., 1998; Hattermann *et al*., 2005). The model has since proven versatile and applicable to a range of situations, from well-gauged areas (e.g. in Germany), to countries with poor data coverage and quality. So far, the SWIM has been applied for river basins in four continents: Europe (Elbe, Rhine, Danube), Asia (Yellow, Jinghe, Tailan, Aksu in China and Ganges in India and Bangladesh), large international rivers in Africa (Blue Nile, Niger, Congo and Limpopo) and South America (Sao Francisco in Brazil) (Hattermann *et al*., 2011; Liersch *et al*., In press; Aich *et al*., 2013; Vetter *et al*., 2013).

The basic spatial structure of the SWIM model has three levels: the catchment, subcatchments and hydrotopes inside the subcatchments (also known as hydrological response units, HRU), which are defined by unique combinations of land cover, soil type and elevation bands within a subcatchment. Spatial input data includes a digital elevation model (DEM) needed for subcatchment delineation and parameterization, land cover and soil maps with an associated soil database. Daily precipitation, temperature (mean, maximum, minimum), relative humidity and solar radiation are required to drive the model.

First, all water components are calculated for each hydrotope and lateral flows are aggregated at subcatchment level. The accumulated subbasin river flow is routed along the river network to the catchment outlet utilizing the Muskingum routing method (Maidment, 1993). The model considers four volumes for each hydrotope: the soil surface, the root or unsaturated zone (divided into 3–10 soil layers in accordance with the soil database) and the shallow and deep aquifers.

At the soil surface, surface runoff is calculated by a modified curve number method (Arnold *et al*., 1990). It is described as a non-linear function of precipitation, snow and glacier melt, depending on soil water content, soil type and land cover type. Potential evapotranspiration is calculated by the Priestley–Taylor method (Priestley and Taylor, 1972) which is used to evaluate actual evapotranspiration depending on the soil water, leaf area index and root depth (Ritchie, 1998). The remaining water infiltrates into the soil column.

Lateral flow in the individual soil layers occurs when field capacity is exceeded after percolation. Return flow to the stream is calculated based on the method described in Smedema *et al*. (2004). Percolation into the shallow aquifer is subject to the delay time function proposed by Sangrey *et al*. (1984).

Snow and glacier melt. As the study region is a high-altitude catchment with 22% glacier coverage, snow and glacier melt are the dominating hydrological processes. As observation data on snow and glacier water resources is generally scarce, the robust degree-day method has been implemented in SWIM and recently extended to include more processes (Huang *et al*., 2013a, b). It includes a continuous description of ice and water content in the snowpack as well as sublimation, refreezing and metamorphism according to the approach of Gelfan *et al*. (2004). Snow and glacier melt processes are very important for the Kumarik catchment, and the usual spatial disaggregation may be not sufficient for mountainous areas. Therefore, 100 m elevation contour bands were used in addition to further split hydrotopes in altitude to allow for a better spatially explicit representation of the snow and glacier melt.

Mean subbasin temperatures are lapse rate corrected to mean hydrotope elevations at run time by:

$$T_h = T_s + \gamma(Z_h - Z_s) \tag{1}$$

where T_h and T_s are hydrotope and subbasin temperature in °C, Z_h and Z_s are hydrotope and subbasin elevation in m, respectively, and γ is the lapse rate that is subject to calibration. The value of γ may vary from -0.5 °C/100 m for humid to -0.98 °C/100 m for dry conditions. Due to the dominantly low humidity in the Tian Shan, it was found to be closer to its drier limit.

Precipitation falls as snow if $T < T_s$. Snow melt M_s is calculated by the degree-day method that has proven to be the most reliable method where accurate information on radiation fluxes is unavailable (Hock, 2005). The degree-day method calculates snow melt by a melting factor δ_s in mm per °C per day when a temperature threshold T_m is exceeded and snow height H_s is greater than 0, as thus stated:

$$M_s \begin{cases} \delta_s(T - T_m), & T > T_m \text{ and } H_s > 0 \\ 0, & H_s = 0 \text{ or } T \le T_m \end{cases} \tag{2}$$

The temperature thresholds T_m and T_s can be adjusted around the freezing point of 0 °C for calibration purposes.

The glacier melt module of the SWIM model also follows the degree-day method similarly to snow melt, but only as a simple linear reservoir. First, initial glacier water equivalents are inferred from individually delineat-

ed glacier areas provided by Bolch *et al.* (2012). An exponential area–volume relationship suggested by Klein and Isacks (1998) is used to estimate the water stored as ice in each hydrotope. The glacier water equivalent depth H_g (mm) is evaluated by:

$$H_g = 4840\rho_i \times A^{0.36} \quad (3)$$

where A is the glacier area and ρ_i the ice density of $0.917\,\mathrm{g\,cm^{-3}}$. The hydrotopes covered by glaciers are assigned this initial H_g. Although this simple estimation of absolute ice volume is associated with considerable uncertainty (Bahr *et al.*, 1997), it provides spatially explicit water depths adequate for discharge simulations.

Glacier melt M_g is calculated by the degree-day approach if the daily mean temperature is above 0 °C and the hydrotope is not covered by snow, as denoted by:

$$M_g = \begin{cases} \delta_g T, & T > 0 \text{ and } H_g > 0 \text{ and } H_s = 0 \\ 0, & \text{otherwise} \end{cases} \quad (4)$$

where δ_g is the melt factor in ($\mathrm{mm\,d^{-1}\,°C^{-1}}$). The melt factor varies between region and glacier, but is generally in the range of 3 – 8 $\mathrm{mm\,d^{-1}\,°C^{-1}}$. It tends to increase with higher solar radiation and elevation, but decrease with higher sensible heat flux and albedo (Hock, 2005). Glacier accumulation occurs from snow that has not melted until September 30, which is defined as the end of the melting period.

Input data processing

The hydrotopes were created from unique combinations of subbasins, land cover and soils and subdivided by 100 m elevation bands. The Kumarik catchment with the final gauge at Xiehela was delineated into 346 subbasins, using the 90 m SRTM digital elevation model (DEM) as shown in Figure 2, with an average area of $37\,\mathrm{km^2}$.

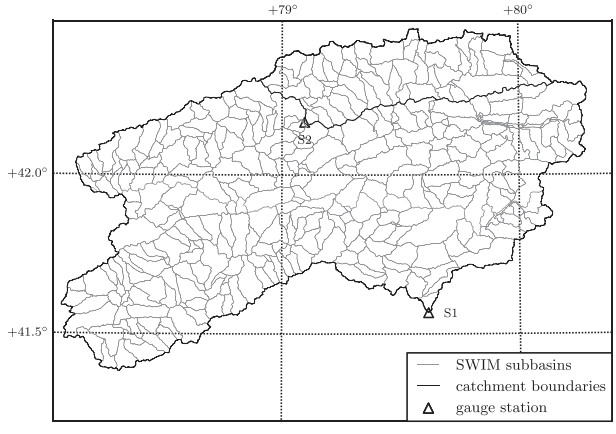

Figure 2. Delineation of the 346 subbasins used by the SWIM model (with an average area of $37.5\,\mathrm{km^2}$)

Merging the two climate data sources (see Table II), the gridded daily data was interpolated to an average subbasin climate using an inverse distance interpolation method and temperature and precipitation lapse rates. The lapse rates (i.e. the temperature and precipitation gradient over elevation) are calculated from the input data for each day. The subbasin precipitation and temperature are again adjusted at run time using the difference in mean subbasin and mean hydrotope elevation and constant lapse rates that serve as calibration parameters. This interpolation chain is schematically shown in Figure 3.

Model calibration and validation

The model was calibrated and validated using observed discharge at the Xiehela station and the internal Kyrgyz station on the Sary-Djaz River using two 12-year periods: January 1, 1964 – December 31, 1975 (calibration) and January 1, 1976 – December 31, 1987 (validation). Two widely used measures of model performance were employed: Nash and Sutcliffe efficiency (NSE, Nash and Sutcliffe, 1970) and relative deviation in water balance (or percent bias). For the Xiehela station, calibration was mainly done visually to avoid misleading analytical performance indicators due to the GLOF events. After an initial manual calibration, the PEST autocalibration algorithm (Doherty, 2003) was used to fine tune model performance. Model calibration and

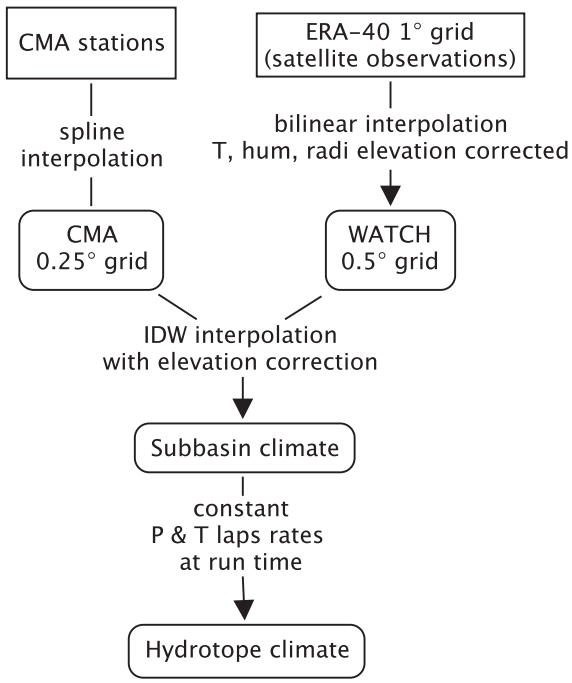

Figure 3. Sources and interpolation steps for the climate data used in the SWIM model for the Kumarik catchment. The ERA-40 data was interpolated to the WATCH grid by Weedon *et al.* (2011)

validation results are given in the sections 'Model calibration and validation' and 'Calibration excluding GLOFs in observations'.

Flood volume estimation using the simulated normal flow

Once GLOF events have been identified, it is possible using the simulated normal discharge and observed discharges to evaluate the flood volume, a proxy for the volume discharged from the Merzbacher Lake.

The form of the GLOF peak hydrograph at the Xiehela station is different from the one directly at the glacier outlet due to river hydraulics. However, water conservation means that the hydrograph area approximately equals the volume of the water exiting the lake during the outburst. The flood hydrograph is separated using the normal catchment discharge simulated by SWIM as baseflow. Earlier studies used graphical hydrograph separation instead (Liu, 1992; Ng *et al*., 2007).

The method of hydrograph separation using the simulated normal discharge is presented in Figure 4. The deviation of observed and simulated discharge at the start and end of the flood period requires the simulated discharge to be first locally corrected, to account for the model uncertainties. The onset ($d_{\nearrow}$) and end ($d_{\searrow}$) dates are variable, but are typically 5 days before and 3 days after the peak date, respectively (Liu, 1992). The simulated discharge is corrected to these dates, as indicated in Figure 4. The deviation in observed and simulated discharge on those days determines the start and end correction factor which is then linearly interpolated for the days in between. This linearly varying correction factor f shown in Figure 4 (bottom) is applied to each day of the GLOF period. After the correction of the simulated discharge, the flood volume is estimated by the difference between the integrated observed and simulated discharge.

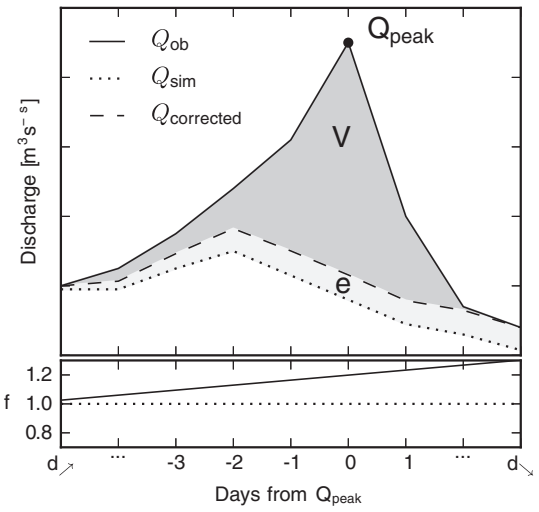

Figure 4. The GLOF hydrograph separation via the corrected simulated discharge $Q_{corrected}$. A linearly varying correction factor f is used to locally correct the simulated Q_{sim}, the area between $Q_{corrected}$ and Q_{sim} is the error e. See explanation in the text

RESULTS

Model calibration and validation

Model performance for the two stations is summarized in Table III. Figure 5 shows observed and simulated discharge for both the calibration and validation periods (only first half of periods shown for better visualization).

For the calibration and validation periods, NSE values of 0.82 and 0.81, respectively, at the Xiehela station indicate a good agreement between simulated and observed discharge. A relatively high negative bias in the water balance, however, shows an average underestimation of between 10% and 16%. The most sensitive model parameters were the temperature lapse rate, the saturated conductivity correction factor, two routing coefficients and snow fall and melt threshold temperatures. This indicates that model uncertainties are largest in the snow and glacier melt periods, as evident in Figure 5.

Closer investigation of the daily discharge dynamics for the Xiehela station shows that large late summer peaks are underestimated in the simulation results while other peaks are slightly overestimated. This simulation mismatch is also reflected by the negative bias in the water balance, suggesting an overall underestimation. An additional analysis is needed to explain these unrepresented peaks. A working hypothesis is that these peaks are caused by the outbursts of the Merzbacher Lake.

In contrast, results for the internal station on the Sary-Djaz River yielded an NSE of 0.82 and 0.8 for the calibration and validation period, respectively, and an acceptable negative bias in water balance of 4–5% was achieved. Considering the much smaller drainage area of this station, the results can be evaluated as satisfactory indicating that the model performs better than at the Xiehela station. As explained above, this station is not located downstream of the Merzbacher Lake catchment, so its discharge record does not contain the GLOF signal.

Table III. Performance statistics for the calibration and validation periods. For station S1, performance is listed for the two cases: with and without GLOFs included in the observations

		Calibration		Validation	
Station	River	NSE	bias [%]	NSE	bias [%]
S1 w GLOFs	Kumarik R.	0.82	−10	0.81	−16
S1 w/o GLOFs		0.90	−2	0.92	−5
S2	Sary-Djaz R.	0.82	−4	0.8	−5

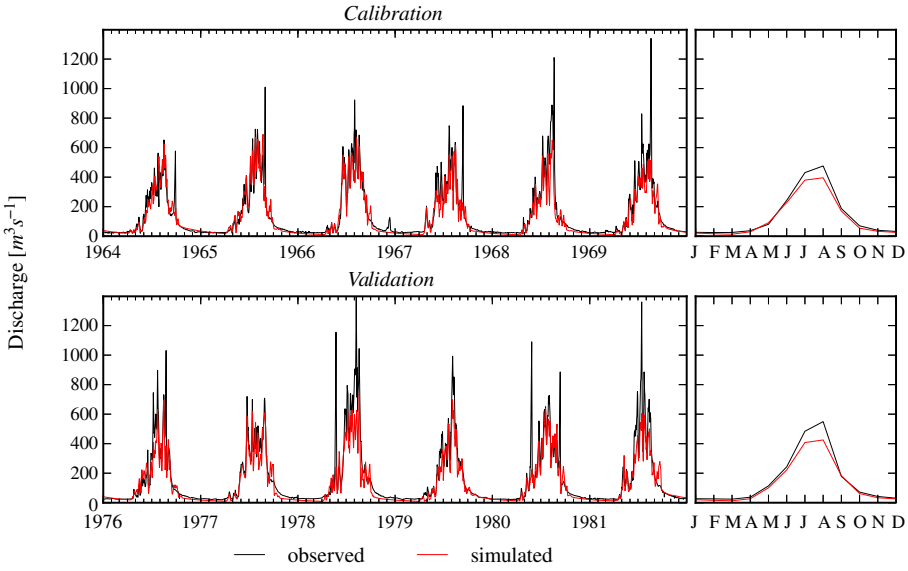

Figure 5. Calibration and validation results with GLOF periods included in the observations: daily dynamics for the first half of the calibration and validation period (left) and average monthly dynamics for the total periods (right)

Unrepresented late summer high peaks

The underestimated peak flow periods at the Xiehela station typically last for 5 to 10 days. During these periods, the model underestimated discharge by between 200 and 1000 m^3s^{-1}. These deviations stand out markedly from the typical model errors and mostly occur in late summer or early autumn.

The search for possible causes, i.e. processes that are not represented in the model, led to the review by Glazirin (2010) of research on the glacier-dammed Merzbacher Lake, as described in the section 'Study site and data'. Glazirin (2010) lists approximate dates and durations of some GLOF events during the period 1931–2005. These are based on a range of different sources including scientific publications and data from glaciologists as well as reports from frontier guards who witnessed these events first hand. It is acknowledged by Glazirin (2010) that sometimes the various sources differ in the reported dates for GLOF events. The GLOF dates given were compared to the underestimated peaks at the Xiehela station. In the period 1964–1987 (the simulation period with available river discharge data), there are 14 years with observed and recorded lake outbursts.

Figure 6 shows selected late summer or autumn peaks for six years not simulated by SWIM, with dates reported by Glazirin (2010) marked. Generally, a good agreement between the reported outbursts and unrepresented peaks is found with a time lag of 5–10 days from the recorded date to the observed peak date at the Xiehela station. Some dates, however, are probably misreported such as in July 4, 1966.

As reported for the catchment earlier (Krysanova *et al.*, 2013, submitted), a high positive and statistically significant correlation was found between the daily temperature (averaged over the catchment) and lagged (by 1–3 days) river discharge at the Xiehela station which breaks over short periods in the end of summer and beginning of autumn. This study concluded that the high (over 95^{th} percentile) flow peaks at the end of summer or beginning of autumn at Xiehela are, to a large extent, caused by the outburst floods from the Merzbacher Lake. For the sub-periods with GLOFs, river flow is not correlated with instantaneous temperature. These high peaks coincide with the unrepresented peaks in the SWIM simulation confirming that they are a result of the regular outbursts from the Merzbacher Lake. As this unique hydrological process is not represented within the SWIM model, it is obvious that the GLOFs cannot be simulated.

An improvement of the model calibration and validation for the Xiehela station requires either the GLOF processes be incorporated into the model or that the GLOF periods are excluded from the observation data. The former option is not currently feasible since the processes leading to the outbursts from the lake are not fully understood and it would require more accurate data on the dynamics of the damming glacier than are available at present. Therefore, the second option was selected.

Calibration excluding GLOFs in observations

The high late summer peaks including their rising and receding limbs which were attributed to GLOF events were excluded from the observation data and the calibration and validation were repeated. This was done for two purposes. First, as the GLOFs have a strong influence on the total river discharge, the hypothesis that excluding GLOFs from the observation data will improve

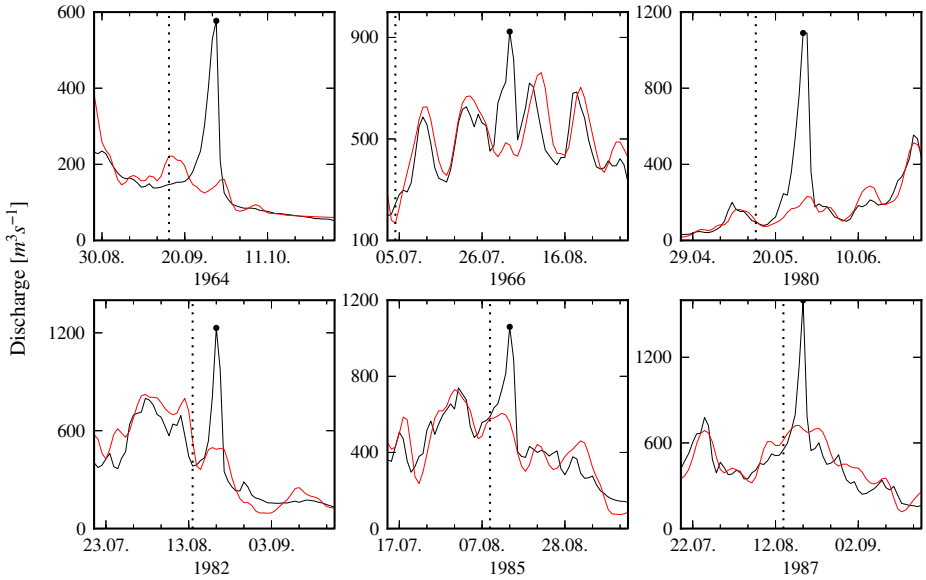

Figure 6. Selected periods with unrepresented peaks in the period 1964–1987: simulated (red) and observed (black) discharge. GLOF dates indicated by Glazirin (2010) are marked with a dashed vertical line

the model performance was tested. Second, the resulting simulated discharge should represent the normal catchment discharge.

A new manual calibration followed by an automatic calibration using PEST rendered a modified parameter set which improved the model performance considerably. Figure 7 shows the calibration and validation results for the Xiehela station after the exclusion of GLOF periods. The model performance was improved: NSE increased to between 0.90 and 0.92 whilst the bias in the water balance declined to between −2% and −5%, in the calibration and validation periods, respectively.

Some deficiencies in the discharge simulation are still apparent in the melt period where some peaks are still slightly underestimated. The same is true for the months of October and November, when discharge tends to be underestimated. However, in general, the results are considered to be good, especially taking into account the quality of the input data.

The simulated normal discharge can be used for the following: (1) to provide a physical basis for the visual interpretation of the GLOF peaks or even to detect GLOFs in the observations for which no reported sightings are available and (2) to act as a baseflow for the separation of the GLOF peaks to estimate the flood volume, a proxy for the volume discharged from the Merzbacher Lake during these events. These two examples are presented in the next two sections.

GLOF identification in observation record

The occurrence of GLOFs, which are not included in the model, can influence modelling performance (as described in section 'Model calibration and validation' for the Kumarik catchment). In the following, an approach is suggested to identify and filter them out. The identification of GLOF events at the Xiehela station could employ the simulated normal discharge and a criterion based on the deviation of this simulated discharge from that in the observational record. This could provide a method to detect GLOFs in the observations that were not reported and to provide a physically based proof for the visually identified GLOFs.

The most basic criterion for the GLOF detection would be to apply a threshold to the observation–simulation residuals (hereafter referred to as residuals), using the non-corrected observations and the normal simulated discharge. That is, asking by what value does the simulation have to deviate from the observed discharge to be identified with a high probability as a GLOF event. As can be seen from the comparison for the total simulation period, most GLOF peak discharges deviate from the simulated normal discharge by more than 500 m^3s^{-1} and up to 1100 m^3s^{-1}.

Simulation residuals are, however, dependent upon the magnitude of observed discharge; this is true for both the GLOF peak discharges and model errors. While typical August GLOFs have peak discharges of above 1000 m^3s^{-1} with typical normal flows of 500–600 m^3s^{-1}, the December GLOF in 1966 peaked at 126 m^3s^{-1} with a residual of 25 m^3s^{-1}. Therefore, the threshold applied to the residuals needs to vary according to the observed discharge. That approach was therefore employed to find this linearly varying threshold empirically using the simulated normal discharge and confirmed GLOFs reported by Glazirin (2010).

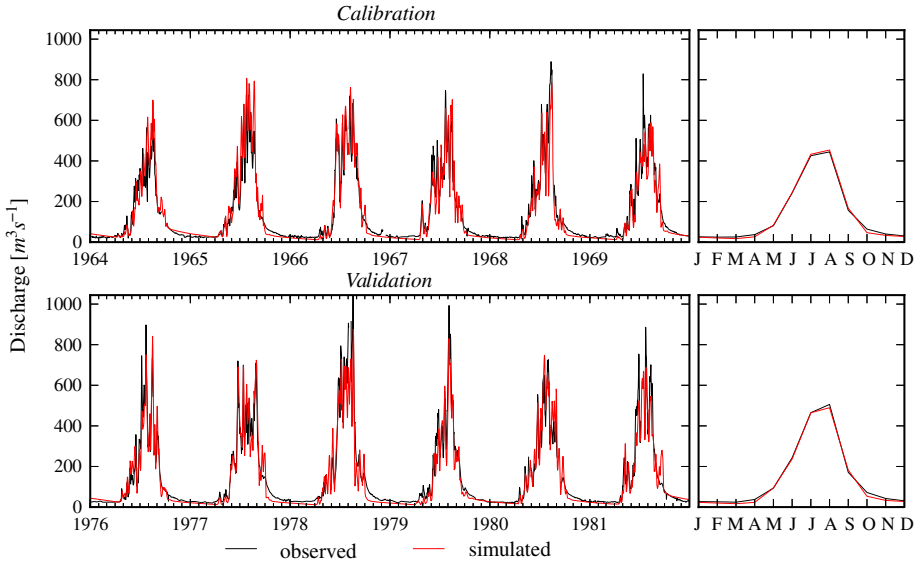

Figure 7. Calibration and validation results without GLOF periods included in the observations: daily dynamics for the first half of the calibration and validation period (left) and average monthly dynamics for the total periods (right)

First, all local (GLOF and non-GLOF) peaks were extracted from the observation data to only consider the maximum discharge without their rising and receding limb. A 10-day moving average filter was used to calculate the discharge anomalies. The maximum discharge of periods during which the anomaly was above the 75th percentile yielded the largest 5–10 peaks in every year, most of them occurring in summer.

The witnessed GLOFs described by Glazirin (2010) were used to find a suitable threshold to discriminate between GLOFs and model uncertainties. A constant threshold of 400 m^3s^{-1} is able to capture most of the reported GLOFs. However, in order to capture the above mentioned non-summer GLOFs, a linear threshold depending on the observed discharge is required.

This was found empirically. The average plus one standard deviation of the ratio between residuals and observations was found as the slope of the linearly varying threshold. To exclude most non-GLOF peaks, a constant component equal to the 75th percentile of the residuals (23 m^3s^{-1}) was used. The following equation describes the varying threshold t_q:

$$t_q = \left(\overline{rq} + \sigma_{rq}\right) \times Q_{obs} + r_{p75} \quad (5)$$

or

$$t_q = 0.434 \times Q_{obs} + 23 \quad (6)$$

where rq is the ratio of residual and observation, $\overline{rq}$ its mean and σ_{rq} its standard deviation and rp_{75} is the 75th percentile of the residuals.

Figure 8 (top) shows the simulation residuals r ($Q_{obs} - Q_{sim}$) against the extracted peak discharges for the modelled period 1964–1987. All GLOFs except one reported by Glazirin (2010) are delineated by this varying threshold. This one peak below the threshold line corresponds to a GLOF on September 1, 1970 with a peak discharge of 721 m^3s^{-1}. This is, however, preceded by a GLOF on July 31, 1970 peaking at 984 m^3s^{-1} (both listed by Glazirin and by Liu). Considering the short time since the last event and the low simulation residual, it is plausible to conclude that this event was misreported.

The GLOF peaks visually identified by Liu (1992) for the same period were included in Figure 8 (bottom). It provides verification that the linearly varying threshold correctly delineates all 25 GLOFs in the observational record and suggests that the threshold line can be used for the identification of GLOFs in other periods.

The method could also be employed for other catchments with glacial lakes in which the same processes lead to intermittent peak discharges associated with GLOFs.

Merzbacher Lake flood volume estimations

GLOF flood volume estimations for the whole simulation period using the method described in the section 'Flood volume estimation using the simulated normal flow' are shown in Figure 9 (black columns). Volumes range from 56 to 291 million m^3 with an average of 167 million m^3. High variability between the volumes is evident, supported by a standard deviation of

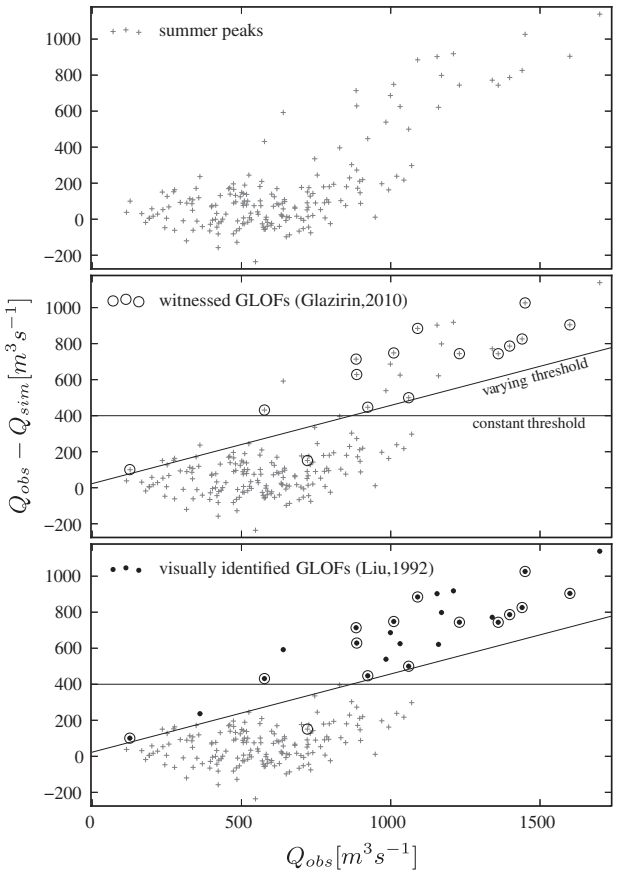

Figure 8. Observed discharge against the observation–simulation residuals for only the extracted summer peaks (top), including GLOFs following reported dates by Glazirin (2010) with the constant ($Q = 400$ m^{2}s^{-1}) and the varying threshold (middle) and including the visually identified GLOF peak discharges by Liu (1992)

55 million m^3. The highest volumes are estimated for the two GLOFs which occurred in May 1978 and 1980 both after years without a GLOF. The lowest volumes are found outside the melting season, e.g. in December, 1966.

Volume estimations without the local correction of simulated discharge are also shown in Figure 9. The large volume differences arise from the model uncertainties before and after the GLOF periods. Relatively small discrepancies between observed and simulated discharge can still lead to large volume changes. For example, a mean underestimation of 70 m^{3}s^{-1} over a typical 8-day GLOF period would lead to an additional 50 million m^3 in volume. These errors are, however, removed through the linear correction while retaining the daily discharge dynamics.

Volumes reported by Liu (1992), also shown in Figure 9 (crosses), vary on average by ±25% from our estimated volumes. Large differences (more than 50%) in estimated volumes exist for three GLOFs: the August, 1985 GLOF volume is 69% higher, while the August, 1978 and July, 1981 events have volumes that are 55% and 72%, respectively, lower than our estimates.

To test the previously reported hypothesis that a correlation exists between the flood volume and baseflow at the Xiehela station (Ng *et al*., 2007), we conducted the same analysis with the derived flood volumes. Results prove this relationship to be existent, but weak with Pearson and Mann–Kendall correlation coefficients both equalling 0.43.

DISCUSSION

There are many glacial lakes in mountainous catchments around the world and their number is increasing, under a general trend of glacier retreat induced by a warming climate (ICIMOD and UNEP, 2001; Huggel *et al*., 2003; Dussaillant *et al*., 2010). Research has been dedicated to identifying those lakes (Bolch *et al*., 2008; Jain *et al*., 2012) and understanding the impacts their potential outbursts might have for riparian communities, infrastructure and ecosystems downstream (Osti and Egashira, 2009; Dussaillant *et al*., 2010; Osti *et al*., 2013). Results presented here address these impacts at catchment scale and provide an approach to both understanding the GLOF impacts as well as analysing them using the simulated catchment discharge with a semi-distributed ecohydrological model, but excluding the GLOFs.

Identifying the Merzbacher Lake GLOFs in the Kumarik catchment using the simulated discharge proved to be useful for several reasons. Although many flood events markedly stand out in the discharge records and could be visually identified, many others occur during the melting season and could well be spring surge events, i.e. temperature induced peaks in glacier melt discharge. This problem was already highlighted in a previous study (Krysanova *et al*., 2013), where discharge correlations with temperature were found to be interrupted. Considering the remoteness and erratic outburst of most glacial lakes, this problem is likely to be common to other discharge records of glaciated catchments.

For example, Osti *et al*. (2013) describe the highly GLOF-prone catchment of the Pho Chu, Bhutan with a total of 549 lakes, eight of which are deemed vulnerable glacial lakes. Finding other flood occurrences by the proposed method would reveal frequencies and magnitudes of smaller outburst floods, though it would not locate their origin. This would also provide proof for large but less documented GLOFs, especially those from ice-dammed lakes that outburst with a degree of regularity but with different magnitudes (e.g. Anderson *et al*., 2003; Dussaillant *et al*., 2010).

Although estimating outburst flood volumes is a routine procedure in most GLOF analyses, it is subject

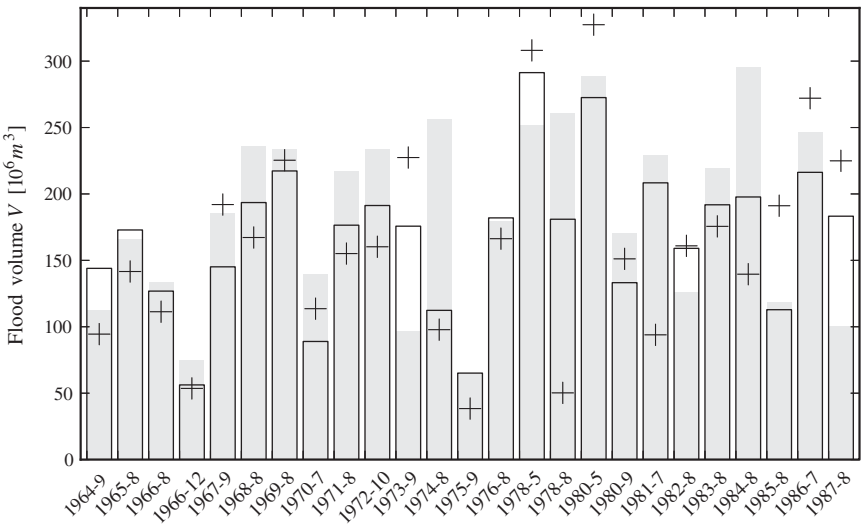

Figure 9. Estimated flood volumes for all GLOF events in the period 1964–1987 derived from corrected (black columns) and uncorrected discharge (light shaded bars) in comparison to volumes estimated by graphical hydrograph separation by Liu (1992) (crosses). Year and month of the peak discharge are given

to several sources of uncertainty, especially where GLOFs are recorded some distance downstream of the lake. Using a hydrological model to simulate the catchment discharge as baseflow during the flood event adds a physical basis to the hydrograph separation. Yet the model uncertainties are propagated, an effect reduced by the correction of the simulated to the observed discharge at the onset and end of the GLOF. Resulting volumes for the Kumarik catchment are comparable to volumes found by Liu (1992) but are generally higher. Huss *et al*. (2007) performed a similar hydrograph separation at hourly time steps using a coupled glacier melt and linear reservoir model at the Gornersee, Switzerland. They benefited from lake volume measurements and were able to quantify the error to ±5–30%. Weighing up between the higher resolved observations in their study and the greater complexity of a process-based model, these error values may apply in the case presented here.

The presented modelling results bring to light how GLOFs are superimposed on normal catchment discharge, which may be relatively low during the event as in 1964 or high during the melting season as in 1987. Hydrological models might therefore be useful in attempts to reconstruct and predict GLOF hydrographs as has been common in GLOF research (Björnsson, 2011). The hydrological model can then serve as a framework for integrated investigations of GLOFs and its impacts downstream under various discharge scenarios, i.e. a first step to modelling GLOF. It also allows simulating the melt water supply to the lake, which has been shown to play an important role in the triggering of a GLOF (Ng *et al*., 2007).

Regarding the modelling of the Aksu catchment in particular, the presented improved model calibration after excluding the GLOFs from the observations is an important step towards a general catchment model of this data scarce environment. Data scarcity, however, still remains a major obstacle to model validation. The availability of observation records in the study region is not satisfactory for a variety of reasons. The Aksu and its tributary catchments are shared by Kyrgyzstan and China (Xinjiang). Due to the international nature of the basin, data are not easily available and shared. Systemic transformations in the region, from centrally planned economies to market economies, have resulted in the shrinkage of environmental monitoring programmes with long time series of records interrupted. Furthermore, the headwater area in high, uninhabited, mountains is difficult to access and poorly gauged. Since there are still only a few gauges in more accessible sites, the representativeness of the available data is questionable and deriving spatial aggregates is uncertain. As there is only patchy information on the glacier mass balance and volume change, uncertainty remains high (see also Krysanova *et al*., 2013, submitted).

CONCLUSIONS

It was demonstrated that GLOFs from the Merzbacher Lake are the plausible explanation of systematic underestimation of simulated river flow during some episodes in late summer and beginning of autumn in the Aksu River. Despite the data scarcity, the implemented SWIM model is able to adequately simulate the complex hydrological processes of the mountainous catchment of the River Kumarik. The GLOFs have a significant impact

on the Kumarik river flow and the overall performance of the model, as was demonstrated by improved model performance after GLOF periods were excluded from the observation data. The NSE was considerably improved and the deviation in water balance was reduced to an acceptable level. It was shown that a catchment model can thereby identify outburst events in hydrological time series, which were not directly observed and are indistinguishable from melt events.

The model-based method to separate the GLOF hydrograph yielded satisfactory results with flood volumes derived ranging from 56 to 291 million m^3. These results are comparable to previous estimates by other authors, but fail to show a stronger correlation with baseflow as was found before by Ng *et al*. (2007). The method developed to estimate the volume of GLOFs can be useful for future research on the hydrology of this and other similar catchments.

GLOFs present a considerable challenge for model-based climate change impact assessments for affected downstream areas. The occurrence and peak discharges of GLOFs cannot be simulated using existing hydrological models fed by the data collected routinely by hydrometeorological monitoring programmes. In these circumstances, the potential to reliably evaluate the impacts of climate change on Merzbacher Lake GLOFs and the whole Aksu catchment is seriously restricted. In order to improve understanding of the processes associated with such events, a dedicated international monitoring and modelling effort would be needed, in both Kyrgyz and Chinese parts of the basin. Such an effort would be required to define the processes leading up to the GLOF events and determine cause–effect relationships. This would in turn enable the explicit incorporation of these hydrologically significant events within hydrological models such as SWIM so that their modified frequency and magnitude under alternative future climates could be investigated.

ACKNOWLEDGEMENTS

This research was funded under the German Federal Ministry for Education and Research (BMBF) project 'SuMaRiO' (Sustainable Land Management of River Oases in the Tarim basin, grant number: 01LL0918J). Dr. Julian Thompson deserves gratitude for valuable comments and corrections.

REFERENCES

Aich V, Liersch S, Huang S, Vetter T, Tecklenburg J, Koch H, Fournet S, Krysanova V, Hattermann FF. 2013. Comparing climate impacts in four large African river basins using a regional eco-hydrological model driven by five bias-corrected Earth System Models. In: Proceedings of the IMPACTS World conference.

Aizen VB, Aizen EM, Melack JM. 1995. Climate, snow cover, glaciers, and runoff in the Tien Shan, Central Asia. *JAWRA Journal of the American Water Resources Association* **31**(6): 1113–1129.

Ajrapetyants SE, Bakov EK. 1971. Morphology of the Merzbacher glacial lake and mechanisms of its catastrophic outbursts. *Some regularities of glacierization of the Tien Shan*. Ilim: Frunse; 75–84 (in Russian).

Anderson SP, Walder JS, Anderson RS, Kraal ER, Cunico M, Fountain AG, Trabant DC. 2003. Integrated hydrologic and hydrochemical observations of Hidden Creek Lake jökulhlaups, Kennicott Glacier, Alaska. *Journal of Geophysical Research: Earth Surface* **108**(F1): 4.1–4.19.

Arnold JG, Allen PM, Bernhardt G. 1993. A comprehensive surface-groundwater flow model. *Journal of Hydrology* **142**(1-4): 47–69.

Arnold JG, Williams JR, Nicks AD, Sammons NB. 1990. *SWRRB: A basin scale simulation model for soil and water resources management*. Texas A & M University Press College Station: TX.

Bahr DB, Meier MF, Peckham SD. 1997. The physical basis of glacier volume-area scaling. *Journal of Geophysical Research* **102**(B9): 20–355.

Björnsson H. 2011. Understanding jökulhlaups: From tale to theory. *Journal of Glaciology* **56**(200): 1002–1010.

Bolch T, Buchroithner MF, Peters J, Baessler M, Bajracharya S. 2008. Identification of glacier motion and potentially dangerous glacial lakes in the Mt. Everest region/Nepal using spaceborne imagery. *Natural Hazards and Earth System Sciences* **8**(6): 1329–1340.

Bolch T, Kutusov S, Li X. 2012. *Updated GLIMS Glacier Database for the Tian Shan*. National Snow and Ice Data Center, Boulder

Doherty J. 2003. PEST: Model Independent Parameter Estimation, User Manual. Tech. rept. Watermark Numerical Computing, Brisbane, Australia.

Dussaillant A, Benito G, Buytaert W, Carling P, Meier C, Espinoza F. 2010. Repeated glacial-lake outburst floods in Patagonia: an increasing hazard? *Natural Hazards* **54**(2): 469–481. 00016.

FAO, IIASA, ISRIC, ISSCAS, JRC. 2011. The Harmonized World Soil Database.

Friedl MA, McIver DK, Hodges JCF, Zhang XY, Muchoney D, Strahler AH, Woodcock CE, Gopal S, Schneider A, Cooper A, Baccini A, Gao F, Schaaf C. 2002. Global land cover mapping from MODIS: algorithms and early results. *Remote Sensing of Environment* **83**(1-2): 287–302. 01071.

Gelfan AN, Pomeroy JW, Kuchment LS. 2004. Modeling forest cover influences on snow accumulation, sublimation, and melt. *Journal of Hydrometeorology* **5**(5): 785–803.

Glazirin GE. 2010. A century of investigations on outbursts of the ice-dammed Lake Merzbacher (Central Tien Shan). *Austrian Journal of Earth Sciences* **103**(2): 171–179.

Gurtz J, Zappa M, Jasper K, Lang H, Verbunt M, Badoux A, Vitvar T. 2003. A comparative study in modelling runoff and its components in two mountainous catchments. *Hydrological Processes* **17**(2): 297–311.

Hattermann FF, Wattenbach M, Krysanova V, Wechsung F. 2005. Runoff simulations on the macroscale with the ecohydrological model SWIM in the Elbe catchment-validation and uncertainty analysis. *Hydrological Processes* **19**(3): 693–714.

Hattermann FF, Weiland M, Huang S, Krysanova V, Kundzewicz ZW. 2011. Model-Supported Impact Assessment for the Water Sector in Central Germany Under Climate Change–A Case Study. *Water Resources Management* **25**(13): 3113–3134.

Hock R. 2005. Glacier melt: a review of processes and their modelling. *Progress in Physical Geography* **29**(3): 362–391.

Huang S, Hattermann FF, Krysanova V, Bronstert A. 2013a. Projections of climate change impacts on river flood conditions in Germany by combining three different RCMs with a regional eco-hydrological model. *Climatic Change* **116**: 631–663.

Huang S, Krysanova V, Hattermann FF. 2013b. Projection of low flow conditions in Germany under climate change by combining three RCMs and a regional hydrological model. *Acta Geophysica* **61**(1): 151–193.

Huggel C, Kääb A, Haeberli W, Krummenacher B. 2003. Regional-scale GIS-models for assessment of hazards from glacier lake outbursts: evaluation and application in the Swiss Alps. *Natural Hazards and Earth System Science* **3**(6): 647–662.

Huss M, Bauder A, Werder M, Funk M, Hock R. 2007. Glacier-dammed lake outburst events of Gornersee, Switzerland. *Journal of Glaciology* **53**(181): 189–200.

ICIMOD, UNEP. 2001. Inventory of glaciers, glacial lakes and identification of potential glacial lake outburst floods affected by global warming in the mountains of Himalayan region. Tech. rept. International Centre for Integrated Mountain Development.

Jain SK, Lohani AK, Singh RD, Chaudhary A, Thakural LN. 2012. Glacial lakes and glacial lake outburst flood in a Himalayan basin using remote sensing and GIS. *Natural Hazards* **62**(3): 887–899.

Jarvis A, Reuter HI, Nelson A, Guevara E. 2007. Hole-filled seamless SRTM data.

Klein AG, Isacks B. 1998. Alpine glacial geomorphological studies in the central Andes using Landsat thematic mapper images. *Glacial Geology and Geomorphology* **10**: 20–41.

Krysanova V, Meiner A, Roosaare J, Vasilyev A. 1989. Simulation modelling of the coastal waters pollution from agricultural watershed. *Ecological Modelling* **49**(1-2): 7–29.

Krysanova V, Müller-Wohlfeil DI, Becker A. 1998. Development and test of a spatially distributed hydrological/water quality model for mesoscale watersheds. *Ecological Modelling* **106**(2-3): 261–289. 00306.

Krysanova V, Wortmann M, Bolch T, Merz B, Duethmann D, Walter J, Huang S, Jiang T, Su B, Kundzewicz ZW. 2013. Analysis of current trends in climate parameters, river discharge, glaciers and land cover in the Aksu River basin (Central Asia). *Hydrological Sciences Journal* submitted.

Liersch S, Cools J, Kone B, Koch H, Diallo M, Reinhardt J, Fournet S, Aich V, Hattermann FF. In press. Vulnerability of rice production in the Inner Niger Delta to water resources management under climate variability and change. *Environmental Science & Policy*. 00003.

Liu J. 1992. Jökulhlaups in the Kunmalike River, southern Tien Shan mountains, China. *Annals of Glaciology* **16**: 85–88.

Liu J, Fukushima Y. 1999. Recent change and prediction of glacier-dammed lake outburst floods from Kunmalik River in southern Tien Shan, China. *Hydrological Extrmes: Understanding, Predicting, Mitigating*. IAHS Publication: Birmingham; 99–107.

Maidment DR. 1993. *Handbook of hydrology*. McGraw-Hill: New York.

Merzbacher G. 1905. *The Central Tian-Shan Mountains 1902-1903*. J. Murray: London.

Moussa R, Chahinian N, Bocquillon C. 2007. Distributed hydrological modelling of a Mediterranean mountainous catchment - Model construction and multi-site validation. *Journal of Hydrology* **337**(1-2): 35–51.

Nash JE, Sutcliffe JV. 1970. River flow forecasting through conceptual models part I – A discussion of principles. *Journal of Hydrology* **10**(3): 282–290.

Ng F, Liu S. 2009. Temporal dynamics of a jokulhlaup system. *Journal of Glaciology* **55**(192): 651–665.

Ng F, Liu S, Mavlyudov B, Wang Y. 2007. Climatic control on the peak discharge of glacier outburst floods. *Geophysical Research Letters* **34**(21): 1–5. L21503.

Osmonov A, Bolch T, Xi C, Kurban A, Guo W. 2013. Glacier characteristics and changes in the Sary-Jaz River Basin (Central Tien Shan, Kyrgyzstan) - 1990-2010. *Remote Sensing Letters* **4**: 725–734.

Osti R, Egashira S. 2009. Hydrodynamic characteristics of the Tam Pokhari glacial lake outburst flood in the Mt. Everest region, Nepal. *Hydrological Processes* **23**(20): 2943–2955.

Osti R, Egashira S, Adikari Y. 2013. Prediction and assessment of multiple glacial lake outburst floods scenario in Pho Chu River basin, Bhutan. *Hydrological Processes* **27**(2): 262–274.

Pieczonka T, Bolch T, Junfeng W, Liu S. 2013. Heterogeneous mass loss of glaciers in the Aksu-Tarim Catchment (Central Tien Shan) revealed by 1976 KH-9 Hexagon and 2009 SPOT-5 stereo imagery. *Remote Sensing of Environment* **130**(Mar.): 233–244.

Priestley CHB, Taylor RJ. 1972. On the Assessment of Surface Heat Flux and Evaporation Using Large-Scale Parameters. *Monthly Weather Review* **100**(2): 81–92.

Ritchie JT. 1998. Soil water balance and plant water stress. *Understanding Options for Agricultural Production*, Systems Approaches for Sustainable Agricultural Development, no. 7, Tsuji GY, Hoogenboom G, Thornton PK (eds). Springer: Netherlands; 41–54.00220.

Sangrey D, Harrop-Williams K, Klaiber J. 1984. Predicting groundwater response to precipitation. *Journal of Geotechnical Engineering* **110**(7): 957–975.

Shen Y, Wang G, Ding Y, Su H, Mao W, Wang S, Duishen MM. 2009. Changes in Merzbacher Lake of Inylchek glacier and glacial flash floods in Aksu River Basin, Tianshan during the period of 1903-2009. *Journal of Glaciology and Geocryology* **31**(6): 993–1002. 00007.

Shi Y, Shen Y, Kang E, Li D, Ding Y, Zhang G, Hu R. 2006. Recent and Future Climate Change in Northwest China. *Climatic Change* **80**(3-4): 379–393.

Smedema LK, Vlotman WF, Rycroft DW. 2004. *Modern Land Drainage: Planning, Design and Management of Agricultural Drainage Systems*. Taylor & Francis: London.

Thevs N. 2011. Water Scarcity and Allocation in the Tarim Basin: Decision Structures and Adaptations on the Local Level. *Journal of Current Chinese Affairs* **40**(3): 113–137. 00008.

Vetter T, Huang S, Yang T, Aich V, Wang X, Gu H, Krysanova V, Hattermann FF. 2013. Intercomparison of climate impacts and evaluation of uncertainties from different sources using three regional hydrological models for three river basins on three continents. In: Proceedings of the IMPACTS World conference.

Wagener T, Wheater HS, Gupta HV. 2004. *Rainfall-Runoff Modelling In Gauged And Ungauged Catchments*. Imperial College Press: London.

Wang G, Shen Y, Su H, Wang J, Mao W, Gao Q, Wang S. 2008. Runoff Changes in Aksu River Basin during 1956-2006 and Their Impacts on Water Availability for Tarim River. *Journal of Glaciology and Geocryology* **30**(4): 562–568.

Weedon GP, Gomes S, Viterbo P, Shuttleworth WJ, Blyth E, Oesterle H, Adam JC, Bellouin N, Boucher O, Best M. 2011. Creation of the WATCH Forcing Data and Its Use to Assess Global and Regional Reference Crop Evaporation over Land during the Twentieth Century. *Journal of Hydrometeorology* **12**(5): 823–848. 00081.

Woesten JHM, Pachepsky YA, Rawls WJ. 2001. Pedotransfer functions: bridging the gap between available basic soil data and missing soil hydraulic characteristics. *Journal of Hydrology* **251**: 123–150.

